This consideration suggests that a search of the low-frequency UVRR spectrum might yield evidence for C-N twisting overtone enhancement.

Conclusions

UVRR spectroscopy of NMA shows the amide bond to be strongly affected by the electron-acceptor (or H-bond donor) properties of its environment, in both the ground and first $\pi-\pi^*$ excited states. The observed affects can be understood as resulting from stabilization of the C=O π^* fragment orbital by electron-acceptor interactions, and the consequent introduction of C-O antibonding and C-N bonding π character into the HOMO. The result is a frequency decrease for the amide I C-O stretching mode which is linearly dependent on the solvent acceptor number, and a frequency increase in the amide II and III modes which share the C-N stretching coordinate. H-bond acceptor interactions at the N-H bond have no affect on the amide frequencies but decrease the N-H stretching frequency in proportion to the solvent donor number. Apparently, the N-H and C=O H-bond interactions are effectively insulated from one another by the $\pi-\sigma$ separation. This insulation makes it possible to evaluate the energetics of C=O and N-H H-bonds independently from spectroscopic data.

The C=O π^* stabilization by electron-acceptor interactions also introduces C-N antibonding character into the first vacant π^* molecular orbital, while retaining C-O antibonding character. Consequently, the excited-state potential is displaced more along the C-N stretching coordinate and less along the C-O stretching coordinate, with the result that amide II and III are intensified, as is amide S via its coupling to amide III, while amide I is weakened. Indeed, in water, amide I shows no resonance enhancement from the first π^* excited state but only from the second, which is mainly a C-O localized state.

The first π^* excited state is also expected to distort by twisting about the C-N bond and to have a minimum energy at a 90° twist angle, thereby providing a pathway for the photoisomerization which is readily observed for NMA via UVRR spectroscopy. This effect should be accentuated by H-bond donor interactions, due to the same orbital composition changes, as is evident from the increasing photoisomerization yield with increasing water content of water/acetonitrile mixtures. The photoisomerization yield decreases with increasing steric bulk of the C and N substituents and is expected to be negligible for polypeptides, except for terminal glycine residues.

While the twisting distortion in the excited state should enhance even quantum transitions of twisting modes in the UVRR spectra, the amide V N-H out-of-plane overtone is undetectable even directly on resonance with the first π^* transition. The likelist explanation is that the change in the C-N torsional force constant is minimized by a barrier to twisting in the excited state and also that the extent of C-N twisting in this mode is relatively small. Low-frequency modes involving out-of-plane displacements of the carbon substituents may be better candidates for overtone enhancement.

Acknowledgment. We thank Professors Krimm and Asher and Professors Garrel and Houk for communicating results of their work prior to publication. This work was supported by NIH Grant GM 25158.

Registry No. NMA, 79-16-3; NEA, 625-50-3; G-G, 556-50-3; G-L, 997-62-6; A-A, 1948-31-8; H_3CCN, 75-05-8; EtOEt, 60-29-7; $H_3C(CH_2)_4CH_3$, 110-54-3; BuOBu, 142-96-1; PhH, 71-43-2; CCl_4, 56-23-5; H_3CNO_2, 75-52-5; EtOH, 64-17-5; $CHCl_3$, 67-66-3; $ClCH_2CH_2Cl$, 107-06-2; $PhNO_2$, 98-95-3; H_3CCOCH_3, 67-64-1; *N*-methylpropionamide, 1187-58-2; *N*-methylisobutyramide, 2675-88-9; *N*-methylpivalamide, 6830-83-7; hexaglycine, 3887-13-6; pyridine, 110-86-1; dioxane, 123-91-1; 2-azacyclotridecanone, 947-04-6; ε-caprolactam, 105-60-2.

Temperature Coefficients of the Rates of Cl Atom Reactions with C_2H_6, C_2H_5, and C_2H_4. The Rates of Disproportionation and Recombination of Ethyl Radicals

Otto Dobis[†] and Sidney W. Benson*

Contribution from Loker Hydrocarbon Research Institute, University of Southern California, University Park, Los Angeles, California 90089-1661. *Received November 5, 1990*

Abstract: Using the very low pressure reactor (VLPR) with recent improvements, we have been able to measure the following rate constants over the range 203-343 K: $Cl + C_2H_6 \xrightarrow{1} HCl + C_2H_5$, $k_1 = (8.20 \pm 0.12) \times 10^{-11} \exp[(-170 \pm 20)/RT]$; $Cl + C_2H_5 \xrightarrow{2} HCl + C_2H_4$, $k_2 = (1.20 \pm 0.08) \times 10^{-11}$; $2C_2H_5 \xrightarrow{3} C_2H_4 + C_2H_6$, $k_3 = (2.00 \pm 0.06) \times 10^{-12}$; $Cl + C_2H_4 \xrightarrow{4} HCl + C_2H_3$, $k_4 = (1.15 \pm 0.13) \times 10^{-10} \exp[-3200 \pm 140)/RT]$. All rate constants are in units of cm³/molecule·s and energies are in cal/mol. Reactions 2 and 3 have no observable temperature dependence over the range measured. Combining k_3 with the experimentally measured value of the ratio of recombination to disproportionation of 0.14 ± 0.01, also independent of temperature, yields for the rate of recombination of ethyl radicals: $k_r = (1.42 \pm 0.11) \times 10^{-11}$. Combining the values of k_4 with the previously measured values of the equilibrium constant K_4 and third law corrected values of ΔS_4 gives for the back reaction: $k_{-4} = (8.7 \pm 0.3) \times 10^{-13} \exp[(-200 \pm 200)/RT]$ and $\Delta H°_{298}(C_2H_3\text{-}H) = 106.0 \pm 0.3$ kcal/mol. The absence of any measurable butane shows that the recombination rate is at least a factor of 400 below its high-pressure value at 3 mTorr. Mass spectral sensitivity data for ethyl radical between 29 and 25 amu is also reported for 20 and 40 eV.

Introduction

Recent improvements[1,2] in the very low pressure reactor (VLPR) have made it possible to study very fast atom-molecule reactions over an extended temperature range, -80 to 200 °C. The reaction of $Cl + C_2H_6$ at room temperature has recently been explored[2] and shown to consist of a number of consecutive and concurrent radical-radical as well as radical-molecule reactions. The entire reaction scheme together with measured rate constants at 298 °K is shown in Scheme I.

[†] Present address: Technical University, H-1521 Budapest, Hungary.

(1) Dobis, O.; Benson, S. W. *Int. J. Chem. Kinet.* **1987**, *19*, 691.
(2) Dobis, O.; Benson, S. W. *J. Am. Chem. Soc.* **1990**, *112*, 1023.

0002-7863/91/1513-6377$02.50/0

Scheme I

$k_{(298)} \times 10^{12}$		
61.0	$C_2H_6 + Cl \xrightarrow{k_1} HCl + C_2H_5$	(1)
12.1	$C_2H_5 + Cl \xrightarrow{k_2} HCl + C_2H_4$	(2)
1.97[a]	$2C_2H_5 \xrightarrow{k_3} C_2H_6 + C_2H_4$	(3)
0.50	$C_2H_4 + Cl \overset{k_4}{\rightleftharpoons} HCl + C_2H_3$	(4)
$(\sim k_2)$	$C_2H_3 + Cl \xrightarrow{k_5} HCl + C_2H_2$	(5)
	$M \xrightarrow{k_{eM}}$ escape from cell	(e)

[a] This value is 10% lower than our reported value,[2] the change arising from a recently discovered error in plotting.

The reaction of Cl atoms with C_2H_4 (step 4) had been studied earlier[3] in a VLPR system where rather larger than expected errors were incurred owing to large background corrections to mass 28 used to measure C_2H_4. In the present study we report on the reactions in Scheme I with better analytical methods and over the range 203–343 K.

While there have been a large number of studies of reaction 1 using various techniques none of the other steps have been measured directly and none of the steps shown in Scheme I have been measured over an extended range of temperatures. Very early studies with VLPR had used inert wall coatings to suppress radical reactions at the walls. These included high-melting (100 °C) chlorofluorocarbon waxes or commercially applied Teflon. These all gave comparable results and did inhibit measurable wall reactions but were restricted in their temperature range. We recently learned how to apply very thin films of Teflon to Pyrex. These thin films are totally transparent and adhere well through many cycles of cooling and heating. They can also be annealed at 250–300 °C to remove any organic plasticizers. With these coated vessels we have never been able to observe any evidence of wall reaction of radicals. By changing residence times by a factor of 6 at constant flow of reactants, using our sliding orifice system, it is possible to measure any changes in reactants or products or in derived rate constants. None have ever been observed, consistent with the absence of wall reactions. Further as we shall show, mass balances on all species including radicals can be made to about 3% and thus preclude any significant wall losses.

Experimental Section

The same turbo-pumped apparatus described earlier[1,2] was used in the present study. It has three interchangeable discharge orifices of 0.193-, 0.277-, and 0.485-cm diameters at the bottom of the reactor cell. They are denoted as ϕ_2, ϕ_3, and ϕ_5, respectively. The unimolecular escape rate constant is k_{eM} $s^{-1} = a_\phi(T/M)^{1/2}$, where T is the absolute temperature, M is the mass of any individual gas component present in the reactor cell, and $a_\phi = 0.285$ for ϕ_2, 0.546 for ϕ_3, and 1.321 for ϕ_5 orifices. For low-temperature runs a refrigerated bath circulator (Neslab ULT-80DD) was connected to the heating/cooling jacket of the reactor cell. Both the short connector tubings and the outer surface of the reactor jacket were isolated from the environment with a heat-insulating cover to keep the reactor temperature within ±0.1 °C even at −70 °C. By changing orifices we can change residence times by a factor of about 5.

Every experiment with a different set of initial chlorine and ethane (RH) concentrations was beam-sampled and repeatedly mass-scanned between m/e 35 and 38 for Cl and HCl analysis at 20 V ionization potential, then, between m/e 25 and 30 for C_2H_6, C_2H_5, C_2H_4, and C_2H_2, both at 20 V and 40-V ionization potentials. After averaging the recorded spectra for each mass, the mass balances were checked and found to be ±2% or better for $[Cl]_0 = [Cl] + [HCl]$ and ±5% or better for $[RH]_0 = [RH] + $ other C_2 species. VLPR uses a chopped molecular beam with a phase-sensitive lock-in amplification that reduces background by factors of 10^3 to 10^4. The resulting signal shows noise of the order of 4%, but this is reduced to 1% by taking averages of some 20–25 consecutive scans at each mass.

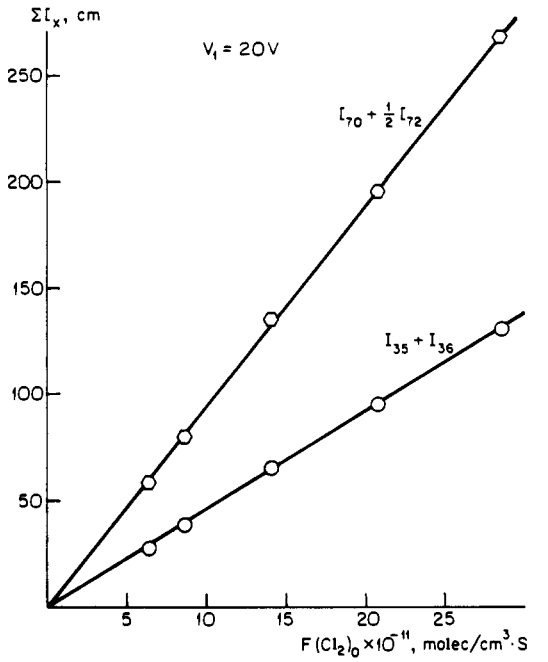

Figure 1. Contribution of ^{35}Cl to mass spectrometer signals of Cl_2 and Cl + HCl with 20-V ionizing electrons at different flow rates of 4.5% Cl_2/He mixture with or without different amounts of initial C_2H_6.

It was possible to calibrate the mass spectrometer signal for Cl_2, Cl, HCl, C_2H_6, C_2H_4, and C_2H_2 using controlled flows of these gases, one at a time. The Cl atom concentration calibration was established by starting with an initially fixed flow of Cl_2 in He and then using mass balances on all Cl-containing species after turning on the microwave discharge. The discharge converted Cl_2 into Cl and HCl (via Cl + H_3PO_4 wall coatings) in a ratio of about 3:1. Figure 1 shows the MS signals for Cl, Cl_2, and HCl.

Since the microwave discharge produces a variable ratio of $(HCl)_0/(Cl)_0$ depending on the initial flow rate of $(Cl_2)_0$, and subsequent chemical reaction of $(Cl)_0$ with excess C_2H_6 can convert in excess of 98% of $(Cl)_0$ into HCl, it is possible to perform very accurate (1%) mass balance determinations on Cl, HCl, and Cl_2. This is illustrated in part in Figure 1 where we plot the total ^{35}Cl content of $(Cl_2)_0$ before the discharge as a function of (Cl_2) flow rate. With the discharge on and the power sufficiently high, no Cl_2 remains and Figure 1 shows the same ^{35}Cl signal now in the form of ^{35}Cl and HCl (36 amu). As can be seen, there is excellent linearity of the plot providing one test of the mass conservation relations. Note that the spectrometer is twice as sensitive to Cl_2 as it is to Cl at 20 V.

Because absolute analytical results are so important to our ability to measure rate constants, we shall take some time to explain our methods.

For Cl_2 it is possible to make up known samples of Cl_2 in He and calibrate the MS signal as a function of flow rate (Figure 1). When the microwave discharge is turned on at an appropriately high power, it is possible to dissociate all of the Cl_2, and MS signals at mass 70, 72, and 74 disappear and we see only signals at masses 35 and 37 from Cl (at 20 eV) and masses 36 and 38 from HCl. (The HCl is formed in the discharge by reaction with H_3PO_4 used to coat the walls to inhibit Cl atom recombination.) It is possible to make an absolute calibration of the MS for HCl by using pure HCl and measuring, at 20 eV, the MS signal at masses 36 and 38. At 20 eV HCl gives negligible signals at masses 35 and 37. We can then assume that all originally introduced Cl_2 produces only Cl atoms and HCl and assign the signal at 35 and 37 to Cl atoms thus estimated and in this way obtain an absolute calibration of the MS for Cl atoms. How reasonable is such an assumption? It can be tested in a variety of ways.

First we can examine the mass spectra of our products and look for any other species produced besides Cl and HCl. We have never found any, searching up to mass 500. But perhaps Cl atoms are being lost in the Teflon or glass or walls of the vessel. If this were the case we should expect with time to see some saturation occurring and a slow increase

(3) Parmar, S. S.; Benson, S. W. *J. Phys. Chem.* **1988**, *92*, 2652.

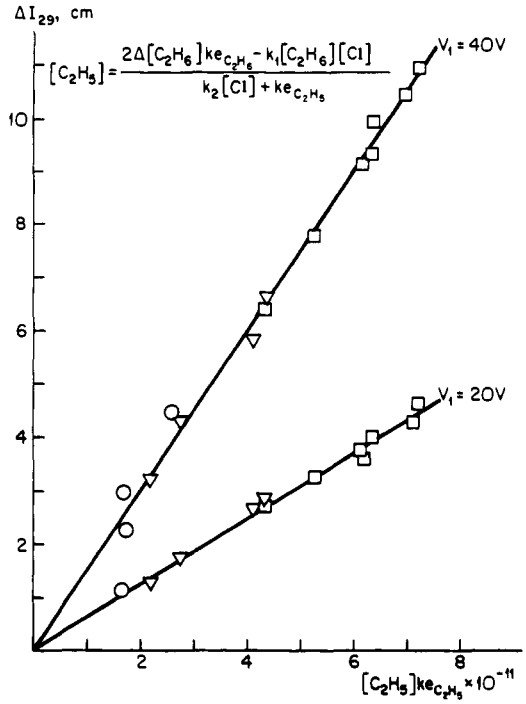

Figure 2. Mass 29 peak measured with 20- and 40-V ionizing electrons (corrected for contribution from C_2H_6) as a function of C_2H_5 flow rate. $\Delta I_{29} = I_{29} - I_{29}(C_2H_6)$. Abscissa are ethyl radical concentrations calculated from eq 6 and multiplied by its escape rate constant to obtain the specific flow rate of C_2H_5. Symbols of orifices: O, ϕ_2; Δ, ϕ_3; □, ϕ_5.

in Cl signal as the system adjusted to a steady state. We have never seen such an effect even after hours of running. When the discharge is turned off or the Cl_2 flow is stopped suddenly, the signals at 35 and 37 decay in complete accord with the Knudsen equation with no signs of a delayed evaporation of Cl or Cl_2 or HCl from the walls of the reactor.

Perhaps more convincing is a typical experiment where we introduce a reactant RH into a flow of Cl + HCl. We see an increase in HCl signal and a decrease in Cl signal. If we interpret these changes as arising from the chemical reaction RH + Cl → HCl + R, then the molecular decrease in Cl must be precisely equal to the increase in HCl. Using our sensitivity for Cl calculated from the Cl_2 flow calibration, we find quantitative agreement (±2%) with this interpretation. This has been tested in every system we have worked with starting with CH_4, cyclopropane, C_2H_4, and C_2H_6. In none of these systems have we ever seen any chlorine-containing species other than HCl.

The ethyl radical spectrum was obtained as described earlier[2] by utilizing 20-V ionizing electrons and observing the mass 29 peak together with the conditions of mass conservation on the sum of all C_2 species. In Figure 2, we show the mass 29 peak of ethyl as a function of calculated ethyl flow at 20 and 40 eV.

In the case of C_2H_6 it is of vital importance to know the absolute concentration of C_2H_5 radicals. This is done in similar fashion to that used for Cl atoms. On introducing known concentrations of C_2H_6 into a steady flow of Cl, we initiate the reaction Cl + C_2H_6 → HCl + C_2H_5. When $(Cl)_0 < 3 \times 10^{11}$ atoms/cm^3 and $(C_2H_6)_0$ is about the same and we use the shorter residence times (ϕ_3 and ϕ_5 orifices), then these are the only reactions which occur in the system and we find decreases in the Cl signal and C_2H_6 mass 30 signal which are equal and equal also to the increase in HCl signal. This gives us good grounds for assigning an absolutely calibrated spectrum to the C_2H_5 radical, assuming that any changes in peaks 29, 28, 27, 26, 25, and 24 when corrected for remaining C_2H_6 must be assignable to C_2H_5. On adding Cl to C_2H_6, we see a decrease in mass 30 signal (C_2H_6) but an increase in mass 29 signal. This can only be due to the C_2H_5 radical. Over a variety of initial conditions, this type of mass balance has been repeatedly verified to within 2%.

Again we have searched the entire mass spectrum looking for recombination species such as C_2H_5Cl, C_4H_{10}, etc., and never found any! Our sensitivity to such species is about 3×10^9 particles/cm^3 as verified by independent calibration on pure samples.

The conservation condition is not quite a simple sum of concentrations over all C_2 species but requires correction to each mass for the slightly different escape rate [$k_{em} \propto M^{-1/2}$; see eq 7–13]. One exception to this is the vinyl radical (V) whose steady-state concentration was calculated from the appropriate kinetic equations. It was, under all our conditions, too small to observe. C_2H_2 also turned out to be too small to observe directly in the presence of the usual large excess of C_2H_4. We are thus confident that the reactions listed represent all (≥96%) of the relevant chemistry in the system.

For species such as Cl, C_2H_5, and C_2H_4 where concentrations can become so extremely low under certain conditions that the mass conservation leads to very high uncertainties, the low concentrations can be calculated with much improved precision from the kinetic equations. An example is the ethyl radical. From the steady-state equations for C_2H_5 (R) we can write

$$(R) = \frac{2\Delta(RH)k_{eRH} - k_1(RH)(Cl)}{k_2(Cl) + k_{eR}} \quad (6)$$

Where $\Delta(RH) = (RH)_0 - (RH)$ and k_{eRH} and k_{eR} are the first-order escape rates of RH and R, respectively, and are both measured and calculated with high accuracy. When k_1 and k_2 are known, and they can be measured directly without needing to know (R), then (R) can be calculated with good precision from eq 6.

In Figure 2 we show the mass 29 signal corrected for (RH) fragmentation plotted against the flux of (R) calculated from eq 6 at both 20- and 40-eV ionizing energies. Note that the lines drawn show a mean scatter of about 2% and, most importantly, go through the origin. The different symbols represent different orifices and hence different residence times and different values for k_{eR} and k_{eRH}.

Equation 6 is derived from the conservation equations which follow (eq 7–13) by multiplying eq 7 by 2 and adding to eq 8.

Treatment of Data

VLPR obeys the condition for a well-stirred reactor in that "mixing time" is established within 1% of the residence time for any species.[4] Since it is a constant flow system, we can write precise steady-state equations for every species. In Scheme I, there are five hydrocarbon species, C_2H_6 (RH), C_2H_5 (R), C_2H_4 (VH), C_2H_3 (V), and C_2H_2 (Ac), and two Cl-containing species, Cl and HCl. The corresponding steady-state equations are

$$C_2H_6: \quad k_{eRH}\Delta(RH) = k_1(RH)(Cl) - k_3(R)^2 \quad (7)$$

$$C_2H_5: \quad k_1(RH)(Cl) = k_{eR}(R) + k_2(R)(Cl) + 2k_3(R)^2 \quad (8)$$

$$C_2H_4: \quad k_2(R)(Cl) + k_3(R)^2 + k_4(V)(HCl) = k_{eVH}(VH) + k_4(VH)(Cl) \quad (9)$$

$$C_2H_3: \quad k_4(VH)(Cl) = k_{eV}(V) + k_4(V)(HCl) + k_5(V)(Cl) \quad (10)$$

$$C_2H_2 \quad k_{eAc}(Ac) = k_5(V)(Cl) \quad (11)$$

$$Cl: \quad k_{eCl}\Delta(Cl) = k_1(RH)(Cl) + k_2(R)(Cl) + k_4(VH)(Cl) - k_{-4}(V)(HCl) - k_5(V)(Cl) \quad (12)$$

$$HCl: \quad k_{eHCl}\Delta(HCl) + k_1(RH)(Cl) + k_2(R)(Cl) + k_4(VH)(Cl) + k_5(V)(Cl) = k_{-4}(HCl)(V) \quad (13)$$

In these equations k_{eM} represents the unimolecular rate constant for the exit of species M through the orifice used. k_{eM} can be measured directly for any given species M at any temperature T. It can also be calculated from the modified Knudsen equation[1] for molecular flow through an orifice. Δ(RH), Δ(Cl), and Δ(HCl) represent the differences in steady-state concentration of the respective species caused by the reaction. Thus in the absence of C_2H_6, $(Cl)_0$ is the initial steady-state concentration of Cl atoms fixed by the flow of Cl_2 into the microwave discharge. On introducing a flow of $(C_2H_6)_0$, both are reduced to new steady-state concentrations (Cl) and (C_2H_6). Some of the Cl_2 introduced into the discharge is converted into HCl rather than Cl. This corresponds to $(HCl)_0$. Since the reaction produces additional (HCl), $\Delta(HCl) = [(HCl)_0 - (HCl)]$ is a negative quantity.

We note that the last two conservation equations, (12) and (13), for (Cl) and (HCl) can be added to give the kinetic equation for mass conservation of (Cl) species:

$$k_{eCl}\Delta(Cl) + k_{eHCl}\Delta(HCl) = 0 \quad (14)$$

(4) Golden, D. M.; Spokes, G. N.; Benson, S. W. *Angew. Chem. Int. Ed. Engl.* **1973**, *12*, 534.

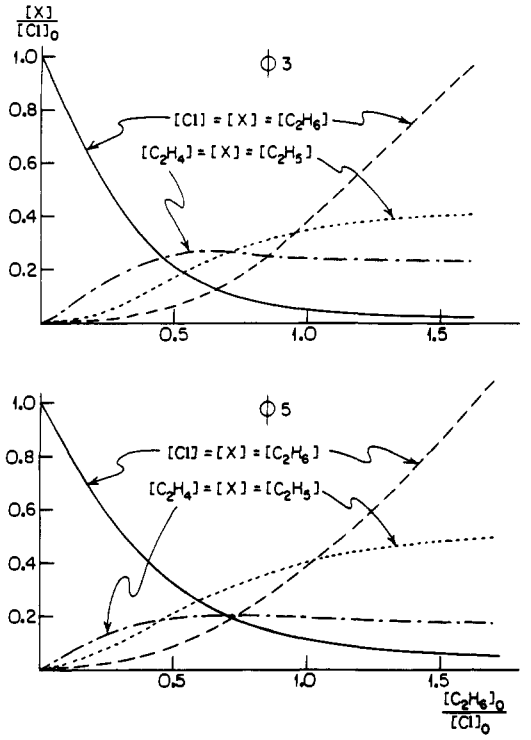

Figure 3. Relative concentrations of Cl, C_2H_6, C_2H_5, and C_2H_4 as functions of $(C_2H_6)_0/(Cl)_0$ at 298 K for ϕ_3 and ϕ_5 orifices.

Since k_{eCl} and k_{eHCl} differ only by $M^{1/2}$ or about 1.5%, this is almost but not exactly equivalent to a simple, static mass balance $\Delta(Cl) + \Delta(HCl) = 0$.

In the same fashion, eq 7–11 can be combined to give

$$k_{eRH}\Delta(RH) = k_{eR}(R) + k_{eVH}(VH) + k_{eV}(V) + k_{eAc}(Ac) \quad (15)$$

Again the exit rate constants k_{eRH} to k_{eAc} span a narrow range of values, varying only by 10%. When all species can be measured independently, eqs 14 and 15 can be used to verify mass balances. When all but one in each set can be measured, then these kinetic conservation equations can be used to deduce the mass spectrum of the unknown species if it is not too small. Finally of the seven conservation equations, we see that only five of them can be considered linearly independent and thus the starting point for deriving rate constants from data.

Every set of initial conditions in VLPR (concentrations of reactants, residence times) reaches a fixed steady state. If we can measure the concentrations of the relevant species present in this stationary state, they can be inserted into the kinetic conservation equations to yield an algebraic relation between the various rate constants.

We have made efforts to detect a signal at mass 27 (20-eV electrons) from the reaction. However, on subtracting contributions from C_2H_6 (very small), C_2H_5 (larger), and C_2H_4 (small), we have been unable to see any residual exceeding background. We thus conclude that (V), the steady-state concentration of vinyl radical, is less than 2% of the other C_2 species. This is in excellent agreement with the value for (V) deduced from eq (10):

$$\frac{(V)}{(VH)} = \frac{k_4(Cl)}{k_{eV} + k_{-4}(HCl) + k_5(Cl)} < \frac{k_4}{k_5} \quad (16)$$

Earlier measurements[3] have shown that at 298 K $k_4 \sim k_{-4}$ while $k_5 \approx 24k_4$, thus fixing the vinyl radical concentration at less than 4% of ethylene. Since the latter is usually less than 20% of the total C_2 species, this confirms our estimates and observations on the smallness of the vinyl concentration. Equation 16 provides a method for calculating vinyl when all the rate constants are known.

Appropriate combinations of the steady-state eq 6–12 leads to the following expression:

$$\left(\frac{k_{eCl}}{k_{eRH}}\right)\frac{\Delta(Cl)}{(Cl)} = \left[\frac{2k_2(Cl)}{k_{eR} + k_2(Cl)}\right]\frac{\Delta(RH)}{(Cl)} + \left(\frac{k_{eR}}{k_{eRH}}\right) \times \frac{k_1(RH)}{[k_{eR} + k_2(Cl)]} + \frac{k_4(VH)}{k_{eRH}}\left[\frac{k_{eV} + 2k_5(Cl)}{k_{eV} + k_5(Cl) + k_{-4}(HCl)}\right] \quad (17)$$

We can also derive

$$k_{eCl}\Delta(Cl) - k_{eRH}\Delta(RH) = k_{eVH}(VH) + 2k_4(VH)(Cl) - 2k_{-4}(V)(HCl) + k_5(V)(Cl) \quad (18)$$

and substituting for $k_4(VH)(Cl)$ from eq 10

$$k_{eCl}\Delta(Cl) - k_{eRH}\Delta(RH) = k_{eVH}(VH) + [2k_{ev} + 3k_5(Cl)](V) \quad (19)$$

and now inserting the steady-state value of (V) from eq 10

$$k_{eCl}\Delta(Cl) - k_{eRH}\Delta(RH) = k_{eVH}(VH) + 2\alpha k_4(VH)(Cl) \quad (20)$$

where

$$\alpha = \frac{k_{eV} + 1.5k_5(Cl)}{k_{eV} + k_5(Cl) + k_{-4}(HCl)} \quad (21)$$

Note that α is virtually insensitive to HCl since $k_5 \sim 22k_{-4}$ and HCl is seldom much larger than 5 (Cl). The result is that α may lie between 0.5 and 1.5 and is usually close to 1.0.

Thus from eq 20 we can solve for (VH):

$$(VH) = \frac{k_{eCl}\Delta(Cl) - k_{eRH}\Delta(RH)}{k_{eVH} + 2\alpha k_4(Cl)} \quad (22)$$

Substituting this in eq 17 yields

$$\left(\frac{k_{eCl}}{k_{eRH}}\right)\frac{\Delta(Cl)}{(Cl)} = \frac{k_1(RH)[k_{eR}/k_{eRH}]}{k_{eR} + k_2(Cl)} + \left[\frac{2k_2(Cl)}{k_{eR} + k_2(Cl)}\right]\frac{\Delta(RH)}{(Cl)} + \frac{\beta k_4}{k_{eRH}}\frac{[k_{eCl}\Delta(Cl) - k_{eRH}\Delta(RH)]}{[k_{eVH} + 2\alpha k_4(Cl)]} \quad (23)$$

where

$$\beta = \frac{k_{eV} + 2k_5(Cl)}{k_{eV} + k_5(Cl) + k_{-4}(HCl)}$$

Note that β is a quantity similar to α and can vary between 0.5 and 2.0. Note also that

$$\beta/\alpha = \frac{k_{eV} + 2k_5(Cl)}{k_{eV} + 1.5k_5(Cl)} \approx \frac{4}{3} \quad (24)$$

When (Cl) $\leq 10^{11}$ particles/cm^3, the term in k_4 can be neglected in eq 22 which then becomes

$$(VH) \approx \frac{k_{eCl}\Delta(Cl) - k_{eRH}\Delta(RH)}{k_{eVH}} \quad (25)$$

which confirms our expectation that C_2H_4 changes significantly with Cl only when both are relatively large (Figure 3). Equation 25, which is a mass conservation relation at low (Cl), provides a convenient method for calculating (VH) when direct observation of mass 28, corrected for contributions from C_2H_6 and C_2H_5 and background N_2, leaves a very small difference.

When the initial ratio of reactants $[C_2H_6]_0/[Cl]_0 \geq 1$, the ratio of $[C_2H_4]/[Cl]_0$ does not change significantly (see Figure 3). For this range of initial concentrations, ethylene concentrations calculated using eq 25 and eq 22 differ by less than 0.5%. Taking the experimental results obtained in that limited range of initial concentration ratios, we can now explore the MS spectra of ethyl radical along with further evidence for the flow balance of all C_2 species when mass fragments of C_2H_4 are taken into account.

Figure 4 shows the fragmentation of ethylene as a function of electron energy used in ionization. With ionization voltages of 40 and 20 V, three and two mass fragments are produced, respectively. The intensities of the parent ions and its ion fragments

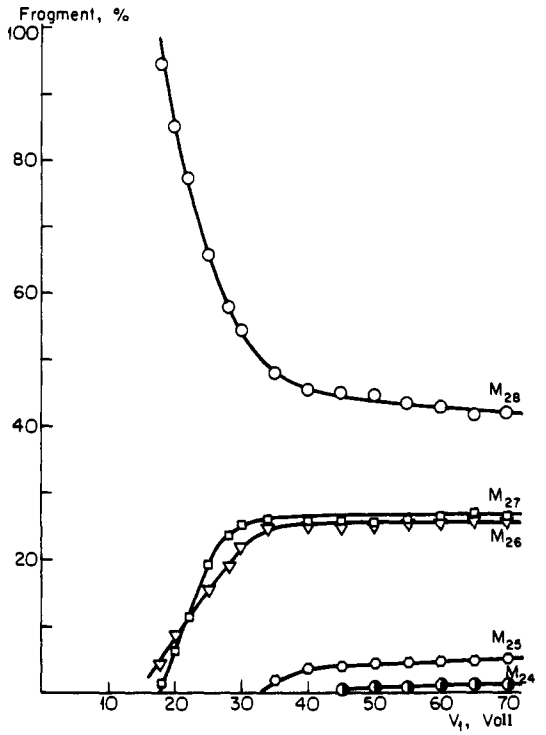

Figure 4. Mass spectra of ethylene as a function of electron energy (abscissa) at 4.23 × 10^{12} molecules/cm^3·s specific flow rate of 50.9% C_2H_4/He mixture. Ordinate: percentage of each mass peak measured between 24 and 28 amu.

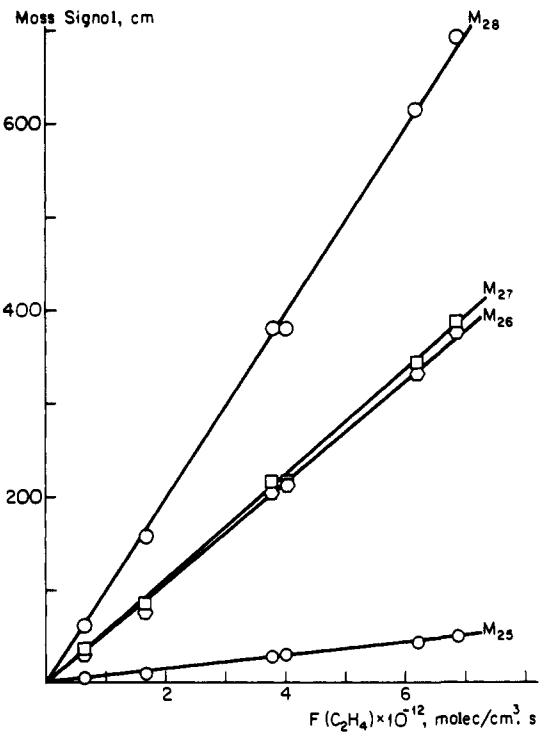

Figure 5. Mass spectra of ethylene recorded at various specific flow rates (abscissa) of 50.92% C_2H_4/He mixture at 40-eV ionization energy.

were recorded at different flow rates of ethylene to obtain MS calibration for C_2H_4 with both 20- and 40-V ionization energies. The latter is presented in Figure 5.

With the knowledge of C_2H_4 concentrations in the limited range $[C_2H_6]_0/[Cl]_0 \geq 1$ and of its escape rate constant, the contribution of ethylene mass signals to each mass peak measured from mass 28 to 25 can now be determined and the residue mass signals be calculated. This is done by subtracting from each peak the contributions due to the known concentrations of C_2H_6 and C_2H_4.

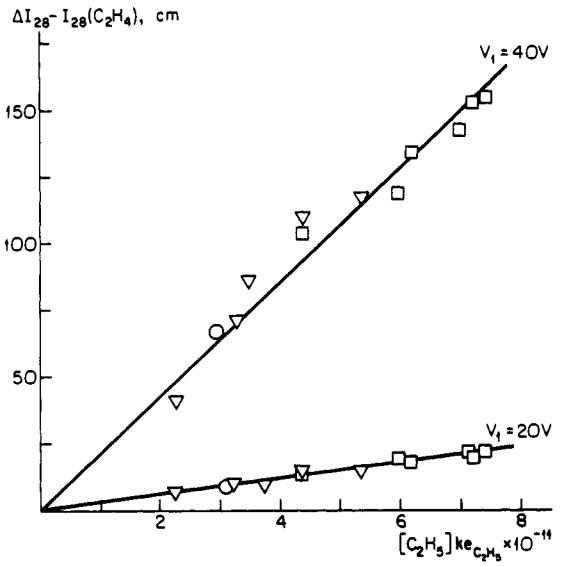

Figure 6. Mass 28 peak measured with 20- and 40-V ionizing electrons and corrected for C_2H_6 and C_2H_4 as a function of C_2H_5 flow rate. $\Delta I_{28} = I_{28} - I_{28}(C_2H_6)$. Symbols of orifices are the same as in Figure 2.

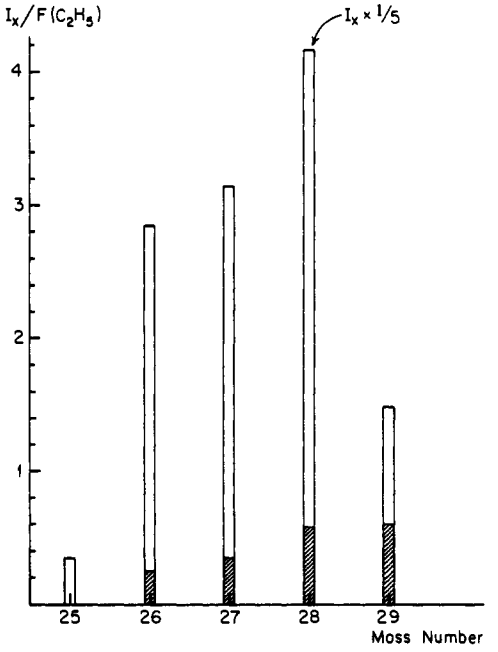

Figure 7. Mass signal intensities per unit flow rate of C_2H_5 obtained for different mass numbers between 25 and 29 amu. I_x is the residue signal intensity (x = mass number) after corrections for C_2H_6 fragment and C_2H_4 contributions. At mass 28, I_x is scaled down by 5. Open bars are spectra at 40 eV; hatched bars are spectra at 20 eV.

The residue is then due to the ethyl radical. The results of such mass signal processing at mass 28 are presented in Figure 6 as a function of C_2H_5 flow rate. We have done the same at amu 27, 26, and 25 although we omit the presentation of data in the interest of conserving space.

The mass signal intensities per unit flow rate of ethyl radicals are shown by the heights of bars in Figure 7. We see that the ethyl radical concentration is 14 times more sensitive at its fragment mass 28 and about twice as sensitive at fragment masses 27 and 26 than to its parent mass at 29. However, comparison of the data in Figures 2 and 6 shows that the scatter is rapidly increasing with decreasing mass. At mass 25 the scatter is ±19%.

Equation 23 is the starting point in obtaining precise values for k_1, k_2, and eventually k_4. But before examining its use in detail, it is instructive to consider Figure 3. Here we have plotted the concentrations of Cl, C_2H_6, C_2H_5, and C_2H_4 all normalized to the initial concentration $(Cl)_0$ as a function of initial $(C_2H_6)_0/(Cl)_0$.

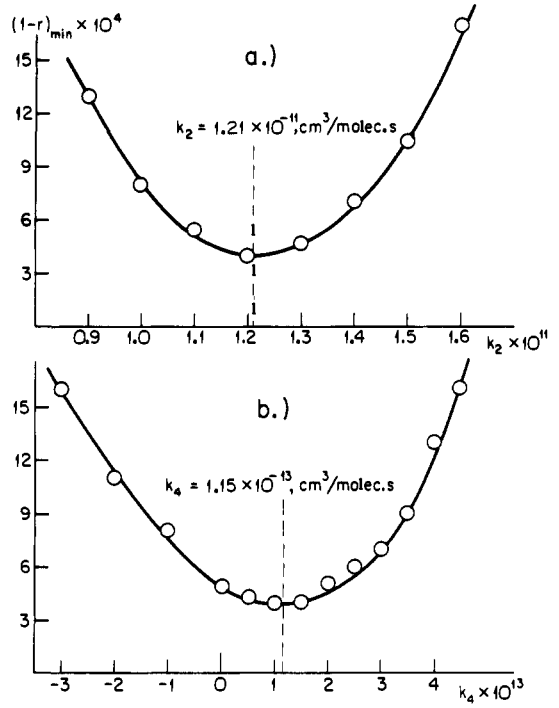

Figure 8. Steps of regression analysis to obtain optimized values for k_2 and k_4 at 233 K. r is the regression coefficient: (a) the sensitivity of eq 23 to k_2, (b) the sensitivity of eq 23 to k_4.

In the typical experiment, we establish a steady flux of Cl atoms through the discharge and then add C_2H_6.

At each fixed flow of $(Cl)_0$ and $(C_2H_6)_0$ we record the concentrations of each species from their mass spectra at the appropriate ionizing voltage. The curves in Figure 3 are calculated from the rate constants at 298 K reported earlier.[2] The upper part of Figure 3 is based on the 3-mm orifice while the lower one is calculated for the 5-mm orifice.

In both parts of Figure 3 we can see that there are three regimes of interest. In the region between $0 < (C_2H_6)_0/(Cl)_0 < 0.5$, C_2H_4 is the dominant hydrocarbon and (C_2H_6) is reduced to very low levels. This is the best region in which to observe the reaction between Cl and C_2H_4 since both are relatively high. Our best values for k_4 come from this region.

The next region of interest is that for $0.5 \leq (C_2H_6)_0/(Cl)_0 \leq 1.1$, where C_2H_5 becomes the dominant hydrocarbon in the system. In this region (C_2H_4) changes very little. This region provides the best data for k_3, k_2, and k_1. Since (Cl) and (C_2H_4) are both relatively low, there is very little of reaction 4 occurring. Finally, there is the last region where $(C_2H_6)_0/(Cl)_0 > 1$. Here C_2H_6 has become the dominant hydrocarbon, (Cl) is relatively low, and reactions 1 and 3 are the dominant reactions.

Figure 8, a and b, illustrates, for the data obtained at −40 °C, the sensitivity of the plot for k_1 to various choices of k_2 and k_4. Note that at −40 °C k_4 is so small that the k_1 plot is not very sensitive to relatively large changes in k_4. In Figure 8a we see that the k_1 plot is much more sensitive to the choice of k_2.

Of particular interest in measuring k_1 is eq 7. This is an exact relation between the species and rate constants. However, since k_1 is so much greater than k_3 ($k_1/k_3 \sim 31$), it turns out that for concentrations of $(C_2H_6)_0$ and $(Cl)_0$ less than 3×10^{11} particles/cm³, the term in $k_3(R)^2$ is less than 1% of the first term and the approximate relation

$$k_{eRH}\Delta(RH) \sim k_1(RH)(Cl) \qquad (7a)$$

gives us a simple and excellent measure of k_1 since all other species are known or measurable.

The use of a larger orifice (ϕ_5) minimizes still further the relatively slow reactions 3, 4, and 5 relative to k_1 and k_2 since the residence time in the reactor is shorter. Conversely, the smallest orifice (ϕ_2) is the best at $(C_2H_6)_0/(Cl)_0 \leq 0.4$ for measurements of k_4.

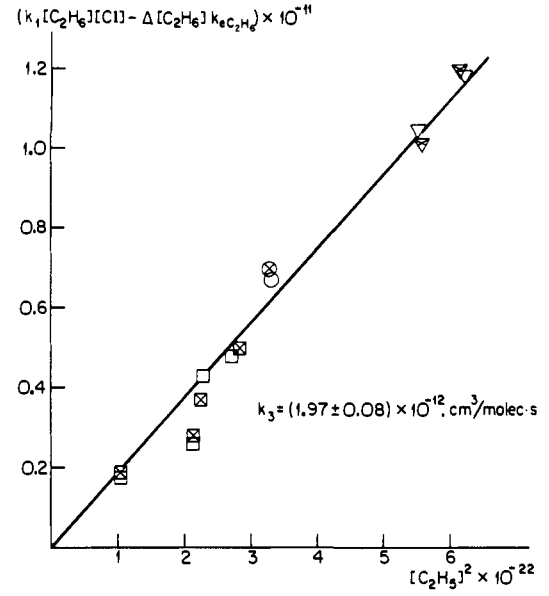

Figure 9. Rate of the ethyl radical disproportionation in reaction 3 as a function of the second power of C_2H_5 concentration plotted according to eq 26 at 298 K. Symbols of orifices are the same as in Figure 2. Crossed symbols mark the data obtained with 20-V while empty symbols show 40-V ionizing electrons.

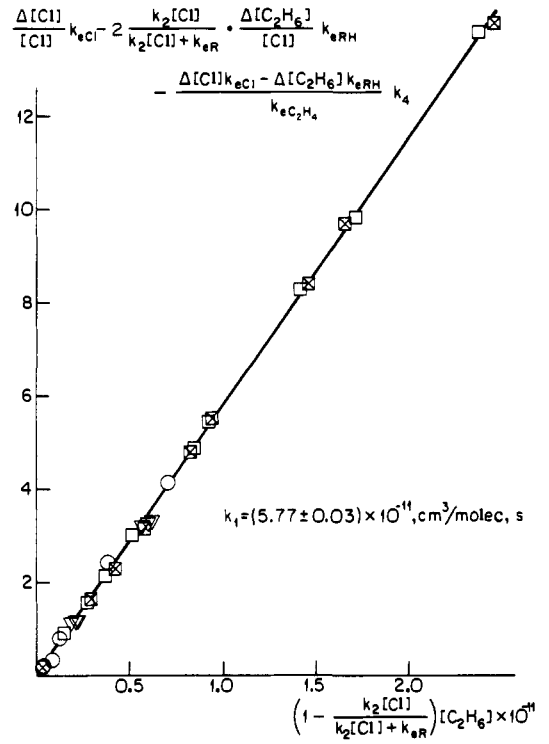

Figure 10. Dependence of relative consumption rate of reactants on ethane concentration plotted according to eq 23 substituted by eq 25 at 233 K. k_2 and k_4 values optimalized in Figure 8 are used for the calculation of ordinate values. Symbols of orifices are the same as in Figure 9.

Equation 6 was used to obtain absolute values of the mass spectra of the ethyl radical. From eq 7 we can write

$$k_1(RH)(Cl) - \Delta(RH)k_{eRH} = k_3(R)^2 \qquad (26)$$

Thus a plot of the left-hand side of eq 26 against $(R)^2$ is used to obtain values of k_3. Figure 9 shows such a plot for the data at 298 K. In figure 10 we show the use of eq 23 to obtain optimum values of k_1 and k_2 from the data at −40 °C.

The usefulness of the different orifices is seen in Figure 3. With the largest orifice (ϕ_5), the residence time is so short that slow

Table I. Some Representative Analytical Data over the Range of Temperatures and Residence Times Explored[a]

T, K	ϕx	V_i, V	$[Cl]_0$	$\frac{[Cl]_0}{[Cl]_0 + [HCl]_0}$	[Cl]	$\frac{[Cl]}{[Cl] + [HCl]}$	$[C_2H_6]_0$	$[C_2H_6]$	$[C_2H_5]$	$I_{29} - I_{29}$-(C_2H_6), cm	$[C_2H_4]$
203	$\phi 5$	40	6.15	0.342	1.26	0.0698	5.15	1.81	2.13	11.2	1.14
203	$\phi 5$	20	6.15	0.342	1.26	0.0698	5.15	1.81	2.12	4.4	1.14
203	$\phi 3$	40	4.67	0.217	0.56	0.0262	4.08	1.41	1.57	3.4	1.06
203	$\phi 3$	20	4.67	0.217	0.56	0.0262	4.08	1.41	1.55	1.2	1.07
203	$\phi 2$	40	21.30	0.351	1.13	0.0186	12.45	1.60	2.96	3.4	7.45
233	$\phi 5$	40	4.54	0.372	0.86	0.0704	4.81	2.12	1.93	10.9	0.70
233	$\phi 5$	20	4.54	0.372	0.86	0.0704	4.81	2.13	1.92	4.6	0.70
233	$\phi 3$	40	6.42	0.322	1.25	0.0627	3.81	0.71	1.42	3.2	1.60
233	$\phi 3$	20	6.42	0.322	1.25	0.0627	3.81	0.70	1.43	1.5	1.59
233	$\phi 2$	40	19.85	0.350	0.91	0.0161	12.25	1.95	3.19	4.5	6.81
268	$\phi 5$	40	5.31	0.340	1.55	0.0992	3.71	1.15	1.63	9.4	0.88
268	$\phi 5$	20	5.31	0.340	1.55	0.0992	3.71	1.15	1.64	4.2	0.87
268	$\phi 3$	40	9.56	0.348	0.91	0.0330	7.23	1.88	2.66	6.3	2.51
268	$\phi 3$	20	9.56	0.348	0.91	0.0330	7.23	1.92	2.66	2.8	2.54
298	$\phi 5$	40	2.33	0.521	0.292	0.0652	5.87	4.17	1.47	9.1	0.184
298	$\phi 5$	20	2.33	0.521	0.292	0.0652	5.87	4.18	1.46	3.6	0.184
298	$\phi 3$	40	5.24	0.297	0.385	0.0218	6.09	2.83	2.08	5.8	1.16
298	$\phi 3$	20	5.24	0.297	0.385	0.0218	6.09	2.81	2.13	2.4	1.14
298	$\phi 2$	40	12.14	0.358	0.308	0.0091	11.69	4.59	3.22	4.5	3.60
298	$\phi 2$	20	12.14	0.358	0.308	0.0091	11.69	4.52	3.39	1.8	3.54
343	$\phi 5$	40	4.54	0.452	1.77	0.1765	2.64	0.75	1.22	8.4	0.60
343	$\phi 5$	20	4.54	0.452	1.77	0.1765	2.64	0.76	1.22	3.4	0.61
343	$\phi 3$	40	12.66	0.379	2.30	0.0687	6.39	0.75	2.07	5.9	3.37
343	$\phi 3$	20	12.66	0.379	2.30	0.0687	6.39	0.75	2.09	2.5	3.37
343	$\phi 2$	40	19.40	0.416	1.92	0.0412	9.58	0.76	2.27	3.4	5.93
343	$\phi 2$	20	19.40	0.416	1.92	0.0412	9.58	0.75	2.29	1.5	5.93

[a] All concentrations are in units of 10^{11} particles/cm^3. ϕx denotes the size of escape orifice (see text). V_i is the ionization voltage used of the MS chamber. $[C_2H_5]$ is calculated according to eq 6. $[C_2H_4]$ is calculated according to eq 22 taking $\alpha = 1$, while, for the last four sets of data at 343 K, α is computed by eq 21 taking $k_5 = k_2$.

Table II. Ranges of Concentrations Used (molecules/cm^3)

	range				$\frac{k_2[Cl]}{k_2[Cl] + k_{eEt}}$
T, K	$[Cl]_0 \times 10^{-11}$	$[C_2H_6]_0 \times 10^{-11}$	$[Cl] \times 10^{-11}$	$[C_2H_6] \times 10^{-11}$	
203	5.12–33.47	1.69–12.45	1.60–9.94	1.02–4.35	0.36–0.94
233	4.20–31.66	1.30–12.25	1.25–11.20	0.38–3.45	0.28–0.93
268	3.07–24.20	1.22–7.57	1.24–2.89	0.49–2.95	0.27–0.80
298	1.70–35.73	0.44–13.17	0.91–8.34	0.29–1.79	0.20–0.986

reactions like (4) contribute very little. To study these with greatest precision, we use ϕ_2 orifice and work in the region of $(C_2H_6)_0/(Cl)_0 < 0.5$.

To return now to eq 23 for obtaining k_1 and k_2, we take our best data from region 3 where $(C_2H_6)_0 > (Cl)_0$ and it turns out that the dominant term on the right-hand side is the first term in k_1 while the second term is relatively insensitive to k_2 and has a contribution $\sim 2\Delta(RH)/(Cl)$ which is measurable with good precision. The third term is completely negligible here. Our procedure is then to plot the left-hand side against (RH). This gives an initial value of k_1 usually to within 10%. We then make an estimate of k_2 and plot the sum of the first two terms. This usually gives an improved value of k_1. We then use a regression program to obtain the values of k_1 and k_2 that produce minimum deviations. Finally an estimate is made of k_4 and the sum of three terms on the rhs of eq 23 is plotted against $\Delta(Cl)/(Cl)$. A regression analysis is then made to give the optimum values of k_1, k_2, and k_4. These are shown in Figure 8 for our data at −40 °C where k_4 has become very small but its contribution is still measurable with precision.

An example of how well the data fit to such a regression analysis is shown in Figure 10 which covers a 50-fold range in the abscissa and 120-fold range in the ordinate. Note that all three orifices fit on the same line which goes through the origin. The mean scatter from the line drawn is less than 1%. We see from Figure 8, a and b, that the data at −40 °C are still very sensitive to k_2 but much less sensitive to k_4 which contributes relatively little except with the ϕ_2 orifice.

In Table II we list the range of concentrations used for $(Cl)_0$ and $(C_2H_6)_0$. Also listed are the measured steady-state concentrations of Cl and C_2H_6. The former varied over a 3- to 9-fold range, while the latter varied over a 40- to 9-fold range. Also shown are the range of values found for the ratio $k_2(Cl)/[k_2(Cl) + k_{eR}]$ which appears in eq 23 and which determines the sensitivity of k_2 measurements. Table III summarizes the values of the rate constants obtained over the temperature range 203–343 K.

Table III. Measured Rate Constants k (cm^3/molecule·s)[a]

T, K	$k_1 \times 10^{11}$	$k_2 \times 10^{11}$	$k_3 \times 10^{12}$	$k_4 \times 10^{13}$
203	5.45 ± 0.07	1.06	2.04 ± 0.05	0.45 ± 0.04
233	5.77 ± 0.03	1.21	2.09 ± 0.06	1.15 ± 0.09
268	5.95 ± 0.06	1.27	2.02 ± 0.04	2.52 ± 0.47
298	6.10 ± 0.11	1.21	1.97 ± 0.08	4.98 ± 0.47
343	6.53 ± 0.17	1.21	1.92 ± 0.06	11.90 ± 0.62

[a] Average: $k_2 = (1.20 \pm 0.08) \times 10^{-11}$; $k_3 = (2.00 \pm 0.60) \times 10^{-12}$.

It would be prohibitive in terms of space to give all of our experimental data since they cover over 200 different initial conditions. However, in Table I we list a representative number of individual steady-state data covering the various orifices and temperatures.

It can be seen in Table III that within the precision of the measurements only k_4 shows a large variation with temperature. k_1 shows a very small but measurable increase with increasing temperature. The two radical–radical disproportionation constants k_2 and k_3 are essentially temperature independent although the latter may be viewed as having a very small activation energy, $E_3 \sim 0.070 \pm 0.040$ kcal/mol.

Figure 11 is an Arrhenius plot of k_4 from which we can write

$$\log k_4(\text{cm}^3/\text{molecule·s}) = -9.94 \pm 0.05 - (3.2 \pm 0.14)/\theta$$

where $\theta = 2.303RT$ in kcal/mol.

In Figure 12 is shown the Arrhenius plot for k_1 over the range measured. The overall variation in k_1 of about 10% over the 140

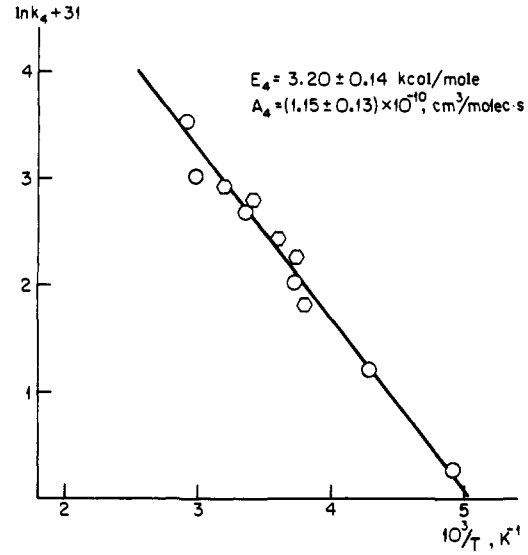

Figure 11. Arrhenius plot of k_4. Hexagons represent the data of ref 3.

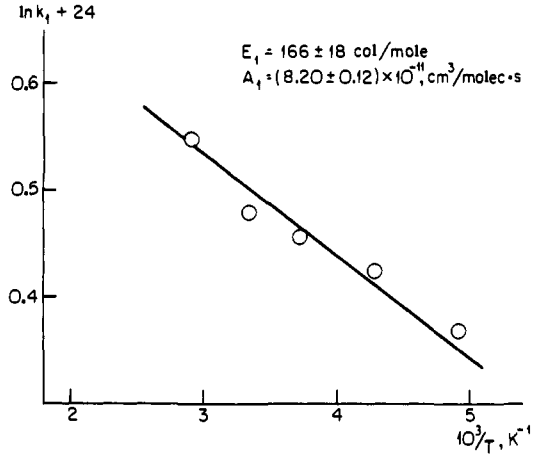

Figure 12. Arrhenius plot of k_1.

K is well outside the precision of measurement of k_1 which varies from 0.5% to 2.5% in this range. The Arrhenius plot yields

$$\log k_1(\text{cm}^3/\text{molecule·s}) = -10.09 \pm 0.01 - (0.166 \pm 0.018)/\theta$$

Discussion

Values for k_1 at 298 K and E_1 measured by different methods are listed in Table IV. They are in excellent agreement with the values found in this study.

We showed earlier[2] that the A factor corresponds very well to that for a tight transition state. Because of its speed, reaction 1 is an excellent source of ethyl radicals, and many authors have made use of it for this purpose.[5,6] In consequence, its accurate value is of interest to many groups. It appears to be in very good standing. Of particular interest is the very small but nevertheless positive activation energy observed by all workers. There have been a number of reports in recent years of negative activation energies involved in the metathesis reactions of halogen atoms or hydrogen halides.[7,8] This does not appear to be the case in the Cl/C_2H_6 system.

Reaction 2, the disproportionation of Cl and C_2H_5 radicals, is actually the high-pressure rate constant for recombination. It has never been measured over an extended temperature range and would be very difficult to measure by techniques other than VLPR. As can be seen in Table III, it shows no variation with temperature. Its contribution to eq 23 is determined by the fraction $k_2(\text{Cl})/[k_{eR} + k_2(\text{Cl})]$. The last column in Table II lists the variation in this fraction over the range of experimental conditions. It varies about 3-fold at most of the temperatures and its contribution to eq 23 is appreciable. We can see in Figure 3 that it will make its greatest contribution when the product of (Cl) and (R) is highest. This occurs when $(C_2H_6)_0/(\text{Cl})_0$ is in the region from 0.5 to 0.9 and $(\text{Cl})_0$ is above 10^{12} particles/cm^3.

If we ignore the 15% decrease in k_2 from 233 to 203 K, the average value over the range can be represented by

$$k_2 = (1.20 \pm 0.08) \times 10^{-11} \text{ cm}^3/\text{particles·s}$$

This value is consistent with a recombination dissociation mechanism:

$$\text{Cl} + \text{C}_2\text{H}_5 \underset{-a}{\overset{a}{\rightleftharpoons}} (\text{C}_2\text{H}_5\text{Cl})^* \xrightarrow{b} \text{HCl} + \text{C}_2\text{H}_4 + 66.7 \text{ kcal/mol}$$

Because step b has a much smaller activation energy (56 kcal) than step −a, step a is rate determining and is paradoxically equal to the high-pressure rate constant although measured under essentially, collision-free conditions. We have already commented earlier[2] that the modified Gorin model[9] overpredicts k_2 by about a factor of 2 at 298 K. It also predicts a roughly $T^{1/6}$ temperature dependence in contrast to the observed T^0 dependence.

It might be expected that k_2 if it is a direct metathesis should be about one-half of k_1 since it has one-half the number of primary H atoms as C_2H_6. However, it is subject to an electronic factor of $^1/_8$ arising from the fact that the products must be formed in singlet states. This suggests that the direct metathesis route $k_{2M} < {}^1/_{16}k_1 \sim 0.3\ k_2$. It contributes less than 25% to the value of k_2.

Radical recombination rates have a large uncertainty associated with their measurement,[10] usually greater than that associated

Table IV. Values Reported for k_1 and E_1

method	$10^{11}k_{(298)}$; cm^3/molecules·s	E_1 (cal)	ref
flow/MS	5.95 ± 0.28		*a*
flow/flow em	4.0 ± 1.2		*b*
flow/flow em	6.0 ± 0.8	121 ± 87	*c*
CCl_4 flash-phot res fl	6.7 ± 0.7		*d*
Cl_2 discharge/res fl	5.7 ± 0.31	266 ± 30	*e*
Cl_2 discharge/res fl	5.7 ± 0.1	180	*f*
VLPR	6.10 ± 0.11	170 ± 20	this work

[a] Ray, G. W.; Keyser, L. F.; Watson, R. T. *J. Phys. Chem.* **1980**, *84*, 1674. [b] Schlyer, D. J.; Wolf, A. P.; Gaspar, P. P. *J. Phys. Chem.* **1978**, *82*, 2633. [c] Manning, G.; Kurylo, M. J. *J. Phys. Chem.* **1977**, *81*, 291. [d] Davis, D. D.; Braun, W.; Bass, A. M. *Int. J. Chem. Kinet.* **1970**, *2*, 101. [e] Lewis, R. S.; Sander, S. P.; Wagner, S.; Watson, R. T. *J. Phys. Chem.* **1980**, *84*, 2009. [f] Baulch, D. L.; Cox, R. A.; Hampson, R. F., Jr.; Kerr, F. A.; Troe, F.; Watson, R. T. *J. Phys. Chem. Ref. Data* **1984**, *13*, 1259.

Table V. Disproportionation/Recombination Ratios for C_2H_5

k_d/k_4	T, K	radical source	ref
0.15	42 0	$C_2H_5CHO + CH_3$	*a*
0.14	350–503	$HCOOC_2H_5 + CH_3$	*b*
0.133	273	$(C_2H_5)_2N_2$(P)	*c*
0.137	344–448	$(C_2H_5)_2CO$(P)	*d*
0.136	312–388	$(C_2H_5)_2CO$(P)	*e*
0.14	298	$C_2H_4/H_2/Hg^*$	*f*

[a] Volman, D. H.; Brinton, E. K. *J. Chem. Phys.* **1954**, *22*, 929. [b] Thynne, F. C. F. *Trans. Faraday Soc.* **1962**, *58*, 676. [c] Dixon, P. S.; Stefani, A. P.; Szwarc, M. *J. Am. Chem. Soc.* **1963**, *85*, 2551. [d] James, D. G. L.; Troughton, G. E. *Trans. Faraday Soc.* **1966**, *62*, 145. [e] Good, A.; Thynne, F. C. F. *Trans. Faraday Soc.* **1967**, *63*, 2708. [f] Falconer, W. E.; Sunder, W. A. *Int. J. Chem. Kinet.* **1971**, *3*, 523.

(5) Slagle, J. R.; Feng, Q.; Gutman, D. *J. Phys. Chem.* **1984**, *88*, 3648. Wagner, A. F.; Slagle, J. R.; Sazynski, D.; Gutman, D. *Ibid.* **1990**, *94*, 1853.
(6) Plumb, J. C.; Ryan, K. R. *Int. J. Chem. Kinet.* **1981**, *13*, 1011. Kaiser, E. W.; Lorkovich, I. M.; Wallington, T. J. *J. Phys. Chem.* **1990**, *94*, 3352.
(7) Seetula, A. J.; Russel, J. J.; Gutman, D. *J. Am. Chem. Soc.* **1990**, *112*, 1347.
(8) Richards, D. P.; Ryther, J. R.; Weitz, E. *J. Phys. Chem.* **1990**, *94*, 3663.
(9) Benson, S. W. *Can. J. Chem.* **1983**, *61*, 881.

Table VI. Recombination of C_2H_5

$k_r \times 10^{11}$ cm³/molecule·s	T, K	radical source method	ref
3.55	349–575	C_2H_6/H_2 discharge	*a*
0.66	415	C_2H_5I/i-C_3H_7I	*b*
4.17	1100	*n*-C_4H_{10} (T)	*c*
0.74	860	$(CrH_5)_2N_2$ (T, VLPP)	*d*
1.40	298	$(C_2H_5)_2N_2$ (P)	*e*
1.99	298	C_2H_6/H flash-photo	*f*
2.06	298	$(C_2H_5)_2N_2$ flash-photo	*g*
1.49	902	C_2H_6 (P)	*h*
1.61	310–370	$(C_2H_5)_2N_2$ (MMS)	*i*
1.48	308	$(C_2H_5)_2N_2$ (MMS)	*j*
1.42	203–343	VLPR	present paper

[a] Avramenko, L. I.; Kolesmikova, R. V. *Acad. Sci. USSR Bull., Div. Chem. Sci.* **1960**, *5*, 755; *6*, 924. [b] Hiatt, R.; Benson, S. W. *Int. J. Chem. Kinet.* **1972**, *4*, 151. [c] Golden, D. M.; Alfassi, Z. B.; Beadle, P. C. *Int. J. Chem. Kinet.* **1974**, *6*, 359. [d] Golden, D. M.; Choo, K. Y.; Perona, M. J.; Piszkiewicz, L. W. *Int. J. Chem. Kinet.* **1976**, *8*, 381. [e] Parkes, D. A.; Quinn, C. P. *J. Chem. Soc., Faraday Trans. 1* **1976**, *72*, 1952. [f] Demissy, M.; Lesclaur, R. *Int. J. Chem. Kinet.* **1982**, *14*, 1. [g] Adachi, H.; Basco, N.; James, D. G. L. *Int. J. Chem. Kinet.* **1979**, *11*, 995. [h] Pacey, P. D.; Wimalasena, J. H. *J. Phys. Chem.* **1984**, *88*, 5657. [i] Arthur, N. L. *J. Chem. Soc., Faraday Trans. 2* **1986**, *82*, 1057. [j] Anastasi, C.; Arthur, N. L. *J. Chem. Soc., Faraday Trans. 2* **1987**, *83*, 277.

with ratios of radical rate constants. In the range 300–500 K, the ratio of disproportionation to recombination for ethyl radicals appears to have a remarkably constant value of 0.14 ± 0.01[10,11] despite the use of diverse techniques for measurement (Table V). While a small positive activation energy for k_3 of about 70 cal/mol can be inferred from the data in Table III, it is just as reasonable, within the precision of the data, to represent k_3 as a constant over the range measured:

$$k_3(\text{cm}^3/\text{molecule·s}) = (2.00 \pm 0.06) \times 10^{-12}$$

With this value and the disproportionation–recombination ratio of 0.14, we can calculate a value for the recombination of ethyl radicals in this range of

$$k_r(\text{cm}^3/\text{molecule·s}) = (1.42 \pm 0.07) \times 10^{-11}$$

This value is listed in Table VI along with some other measurements. Our value agrees with these within the listed precisions and we feel that it is the most accurate.

The simplest and most direct method for the measure of k_4 is by observation of the reaction of Cl with C_2H_4. This is a relatively simple kinetic system with only the fast reaction of Cl + vinyl → C_2H_2 + HCl as a complication. This system together with the measurements of the equilibrium constants K_4 has been reported.[3] It leads to a value for k_{-4} from the relation

$$k_{-4} = k_4/K_4$$

The rate constants k_4 from this earlier study showed a precision of about 10–12% while the precision of K_4 ranged from 14 to 18%.

Despite the greater complexity of the present system, we are able to obtain as good or better precision in our measure of k_4. We can see from Figure 3 that in the range of concentrations $(C_2H_6)_0/(Cl)_0 < 0.5$, residual C_2H_6 and C_2H_5 are both so low that only C_2H_4 is an important reaction source for the still relatively high (Cl). Reaction 1 is about 120 times faster than step 4, and even step 2 is 24 times faster so that little C_2H_6 or C_2H_5 will remain when Cl + C_2H_4 begins to occur.

Our experimental values for k_4 (Table III) are well described by an Arrhenius plot (Figure 11) and can be represented by

$$k_4(\text{cm}^3/\text{molecule·s}) = (1.15 \pm 0.13) \times 10^{-10-(3.20\pm0.14)/\theta}$$

For comparison we show the data of ref 3 (hexagons) in the same plot. We have not included these in the calculation of the Arrhenius parameters, but we note that they fit on our Arrhenius line quite well with about the same precision. The largest deviations occur at the lowest (263 K) and highest (338 K) temperatures used in this study. It is only at 338 K that k_4 falls seriously below our plot by some 40%.

The Van't Hoff plot of K_4 in the earlier study[3] led to values of $\Delta H°_4 = 3.3 \pm 0.4$ kcal/mol and $\Delta S°_4 = 11.4 \pm 1.3$ cal/mol·K. This latter leads to 58.6 ± 1.2 cal/mol·K for S_{298}(vinyl) which is higher than the statistical calculations or empirical methods (based on comparisons with C_2H_4 and CH_2O) yield. Using a preferred value of 57.0 cal/mol·K for S_{298}(vinyl) and an actual upper limit, the preferred, third law values of $\Delta H°_{4(298)} = 3.0 \pm 0.4$ and $\Delta S°_{4(298)} = 9.7 \pm 0.5$ were reported. If we combine these with our current value for k_4 we can calculate

$$K_4 = 132 \times 10^{-3.0/\theta}$$

$$k_{-4}(\text{cm}^3/\text{molecule}) = 8.7 \times 10^{-13-0.2/\theta}$$

The estimated uncertainty in k_{-4} is about 15% over the entire range. The value of $\Delta H°_{4(298)} = 3.0$ kcal/mol leads to a value of $\Delta_f H°_{(298)}$(vinyl) = 66.4 ± 0.4 kcal/mol and a bond strength in ethylene of $DH°_{298}(C_2H_3\text{–H}) = 106.0 \pm 0.4$ kcal/mol. This is in the middle of the range of values which have been reported.[12]

There have been two different, direct studies of k_{-4}. In the first of these,[13] C_2H_3I (VI) was dissociated by a short intense laser pulse at 248 nm to produce ~83% C_2H_3 + I and ~17% C_2H_2 + HI. The production of C_2H_4 was followed by its IR absorption at 3132 cm^{-1} using a finely tuned diode laser. (VI) ~10^{16}, (HCl) ~ 10^{17}, and (C_2H_6) (for quenching) ~10^{17} particles/cm³. The half-life for C_2H_4 production was found to be about 3–5 μs and yielded from the assumed three-step mechanism a value of $k_{-4} = (13 \pm 3) \times 10^{-13}$ at 298 K, about 2.6-fold higher than that reported here. The authors found that about 25% to 40% of their vinyl radicals were removed by a reaction other than (–4) which they attributed to a VI, non-C_2H_4 producing reaction, possibly quenching. Note that excited V* produced by the laser can undergo only about 10^2 collisions with C_2H_6 in 3 μs. They are produced with a photon of about 115 kcal to break a 65-kcal bond. This leads to 50 kcal of excess energy to share between I and V. The former can have at most 23 kcal of electronic excitation and so there must be >27 kcal of vibrational energy in the excited V*. It is possible that V* reactions play a role either by reaction with C_2H_6 or even VI. They may also contribute to the IR absorption used to analyze for C_2H_4.

In the second study,[14] a pulsed laser photolysis (using 193 nm) of C_2H_3Br(VBr) was used to generate low concentrations (<10^{11}) of V + Br in a flow system of He + HCl at about 1 Torr. The authors reported $k_{-4} = (20 \pm 2) \times 10^{-13}$ cm³/particle·s at 298 K, a value about 4-fold larger than the value reported here. More importantly, they find a negative activation energy $E_{-4} = -0.67 \pm 0.23$ kcal/mol over the range 300–500 K, directly at variance with our positive value of 0.20 ± 0.4 kcal/mol. These are very carefully done experiments, and the authors have gone to great lengths to test the system for various possible artifacts. Most interesting is the fact that they also use coated vessels with Teflon and halocarbon coatings very similar to those used in our experiments. The major difference from the VLPR technique is that they use a pulsed-flow system. To obtain rate constants they must integrate kinetic equations over time. VLPR is a well-stirred reactor in steady state. It is conceivable that there are transient effects at the walls, in the flow experiments which are triggered and started at each laser pulse which differ from the steady-state VLPR experiments where no transients occur.

(10) *CRC Handbook of Bimolecular and Termolecular Gas Reaction*; Kerr, J. A., Ed.; CRC Press: Boca Raton, FL, 1981; Vol. 2, p 80.
(11) Reid, L. E.; LeRoy, D. J. *Can. J. Chem.* **1968**, *46*, 3275. Pacey, P. D.; Wimalasena, J. H. *Ibid.* **1984**, *62*, 293.
(12) Ayranci, G.; Back, M. H. *Int. J. Chem. Kinet.* **1983**, *15*, 83. McMillen, D. F.; Golden, D. M. *Annu. Rev. Phys. Chem.* **1982**, *33*, 493.
(13) Krueger, H.; Weitz, E. *J. Chem. Phys.* **1988**, *88*, 1608.
(14) Russell, J. J.; Senkan, S. M.; Seetula, J. A.; Gutman, D. *J. Phys. Chem.* **1989**, *93*, 5184.
(15) Back, R. A.; Griffiths, D. W. L. *J. Chem. Phys.* **1967**, *46*, 4839. These authors have shown persistence of excited vinyl radicals at up to 20 Torr of C_2H_4.

The same questions of vibrational excitation and quenching arise. The 193-nm photon has about 150 kcal and breaks a 75-kcal bond. Hence 75 kcal of internal excitation is shared between V* and Br*. The latter cannot have more than 10 kcal of electronic excitation so that V* may share 65 kcal with Br. Their half-life, using $\sim 10^{14}$ HCl is, about 1.5 ms and is measured by their loss, not by C_2H_4 production. It is difficult to know what role excited V* plays in their system, either in the chemical reaction or in the mass spectrometer detection where threshold photoionization is used to produce mass 27 cations. In 1.5 ms there are about 2500 collisions of V* with He, a very poor vibrational quencher. Most disconcerting is the fact that a rate constant of about 100 s^{-1} is attributed to some unknown wall reaction of vinyl radicals. This accounts for from 25 to 50% of the total loss of vinyl.

In the VLPR system, all species are under observation and mass balances can be done to a few percent on all species. This is not the case in the flow systems where unknown wall reactions remove up to half of the radicals in times competitive with the reaction times.

The carrier gas He is a notoriously poor quencher of vibrational energy, particularly for species with small excitations in any given mode. Hence there is very little guarantee that one is not dealing with vibrationally excited radicals. This internal energy may affect their reactivity and also their detectability in the mass spectrometeric system which depends on threshold photoionization to produce ions. It may be that excited radicals have a larger ionization cross-section than ground-state species. In this case, there could be a systematic bias in detectability as initially produced radicals are collisionally quenched during the course of the reaction. This could contribute to the mysterious wall loss of radicals. Such an effect could also show a systematic variation with temperature.

If in our system radicals disappeared on the walls with rates comparable to this, we should never have seen ethyl radicals, and none of the subsequent reactions reported would have occurred. In our 2-mm orifice, residence times of radicals are about 2 s so that wall rates of 10–200 s^{-1} would have precluded observations of any radicals or radical reactions.

In the earlier Cl/C_2H_4 study[3] where equilibrium was observed by adding HCl, some studies were made with an initial ratio $(HCl)_0/(Cl)_0 \sim 2.2$, and (Cl) consumption was followed to extents of 50% and 60%. This would not have been possible if k_{-4} were two to four times larger than we have measured. In this equilibrium study there would have to have been collective errors in the concentrations of C_2H_4, Cl, and HCl amounting to 400 and 200% for such an error to occur. This is simply not possible in view of the excellent mass balances observed.

Acknowledgment. This work has been supported by a grant from the National Science Foundation (CHE-8714647).

Registry No. Cl, 22537-15-1; C_2H_6, 74-84-0; C_2H_5, 2025-56-1; C_2H_4, 74-85-1; H, 1333-74-0.

Langmuir–Blodgett Film Assembly of Novel Dye Molecules Substituted by a Steroid Skeleton: Molecular Design for Uniform Films

Katsuyuki Naito,* Akira Miura, and Makoto Azuma

Contribution from the Advanced Research Laboratory, Toshiba Research and Development Center, Toshiba Corporation, 1 Komukai-Toshiba-cho, Saiwai-ku, Kawasaki 210, Japan.
Received January 23, 1991

Abstract: Amphiphiles including dye skeletons such as 7,7,8,8-tetracyanoquinodimethane (TCNQ), *p*-phenylenediamine (PD), *p*-quinonediimine (QI), tetrathiafulvalene (TTF), *p*-benzoquinone (BQ), and anthraquinone (AQ) were newly synthesized to obtain a design rule to produce uniform LB films. The amphiphiles were divided into four groups, based on the differences in hydrophobic tails: monoalkyl derivatives (group 1); *tere*-dialkyl or *tere*-tetraalkyl derivatives (group 2), where long alkyl chains were attached to the dye skeleton at separate locations; *ortho*-dialkyl derivatives where two alkyl chains were attached to the dye skeleton at adjacent locations (group 3); and steroid derivatives (group 4). The amphiphiles including large dye moieties in groups 1 and 2 generally formed unstable monomolecular films on a water surface, if their hydrophilic properties were weak. The latter two groups, whose hydrophobic tails could be closely packed together, yielded stable and condensed monomolecular films. The films for group 3, however, indicated high surface viscosity values (>1 g/s at 10 dyn/cm), resulting in inhomogeneous LB films. Group 4 molecules yielded less viscous films, resulting in homogeneous LB films. Furthermore, introducing a large and/or strong hydrophilic head into group 3 or 4 compounds was effective for decreasing the viscosity values (10^{-1}–10^{-2} g/s) and producing homogeneous LB films. The geometric sizes and molecular cohesions of the amphiphiles were found to have great influence on the film-forming properties. Optimum molecular structures for producing uniform dye LB films were discussed.

Introduction

The Langmuir–Blodgett (LB) method[1] has long been known as a technique for use in constructing organic thin films with high-order molecular arrays or superlattices with different kinds of molecules. A wide range of applications using LB films, including various functional molecules, have been proposed.[2] However, the presence of structural inhomogeneities and microdefects in the built-up films on metal or semiconductor substrates has recently been revealed.[3] Furthermore, LB films are rather

(1) (a) Adams, N. K. *The Physics and Chemistry of Surfaces*; Dover: New York, 1968. (b) Adamson, A. W. *Physical Chemistry of Surfaces*; John Wiley & Sons: New York, 1982.

(2) For example, see: (a) Swalen, J. D.; Allara, D. L.; Andrade, J. D.; Chandross, E. A.; Garoff, S.; Israelachvili, J.; McCarthy, T. J.; Murray, R.; Pease, R. F.; Rabolt, J. F.; Wynne, K. J.; Yu, H. *Langmuir* **1987**, *3*, 932. (b) Ahmed, F. R.; Burrows, P. E.; Donovan, K. J.; Wilson, E. G. *Synth. Met.* **1988**, *27*, B593. (c) Girling, I. R.; Kolinsky, P. V.; Cade, N. A.; Earls, J. D.; Peterson, I. R. *Opt. Commun.* **1985**, *55*, 289. (d) Blinov, L. M.; Dubinin, N. V.; Mikhnev, L. V.; Yudin, S. G. *Thin Solid Films* **1984**, *120*, 161. (e) Roberts, G. G. *Contemp. Phys.* **1984**, *25*, 109.

0002-7863/91/1513-6386$02.50/0